



HAL
open science

One-pot preparation of iron/alumina catalyst for the efficient growth of vertically-aligned carbon nanotube forests

Arthur Roussey, Nicolas Venier, Hussein Fneich, Lucas Giardella, Thomas Pinaud, Said Tahir, Mario Pelaez-Fernandez, Raul Arenal, Ahmad Mehdi, Vincent Jourdain

► To cite this version:

Arthur Roussey, Nicolas Venier, Hussein Fneich, Lucas Giardella, Thomas Pinaud, et al.. One-pot preparation of iron/alumina catalyst for the efficient growth of vertically-aligned carbon nanotube forests. *Materials Science and Engineering: B*, 2019, 245, pp.37-46. 10.1016/j.mseb.2019.05.005 . hal-02133685

HAL Id: hal-02133685

<https://hal.science/hal-02133685>

Submitted on 22 Oct 2021

HAL is a multi-disciplinary open access archive for the deposit and dissemination of scientific research documents, whether they are published or not. The documents may come from teaching and research institutions in France or abroad, or from public or private research centers.

L'archive ouverte pluridisciplinaire **HAL**, est destinée au dépôt et à la diffusion de documents scientifiques de niveau recherche, publiés ou non, émanant des établissements d'enseignement et de recherche français ou étrangers, des laboratoires publics ou privés.



Distributed under a Creative Commons Attribution - NonCommercial 4.0 International License

1 **One-pot preparation of iron/alumina catalyst for the efficient growth of vertically-**
2 **aligned carbon nanotube forests**

3
4

5 Arthur Roussey,^{a,f} Nicolas Venier,^a Hussein Fneich,^b Lucas Giardella,^c Thomas Pinaud,^b Saïd
6 Tahir,^c Mario Pelaez-Fernandez,^d Raul Arenal,^{d,e,g} Ahmad Mehdi^b and Vincent Jourdain^{c,*}

7
8

^a Global Technologies, 496 avenue Francis Perrin, Rousset, France

9 ^b Institut Charles Gerhardt, UMR5253 CNRS, ENSCM, Université Montpellier, Place Eugène
10 Bataillon, 34095 Montpellier Cedex 05, France

11 ^c Laboratoire Charles Coulomb, CNRS, Univ. Montpellier, Montpellier, France

12 ^d Laboratorio de Microscopias Avanzadas (LMA), Instituto de Nanociencia de Aragon (INA),
13 Universidad de Zaragoza, C/ Mariano Esquilor s/n 50018 Zaragoza, Spain

14 ^e ARAID Foundation, 50018 Zaragoza, Spain

15 ^f Present address: Grenoble Alpes University, CEA-LITEN, 17 rue des Martyrs, 38054
16 Grenoble Cedex 09, France

17 ^g Instituto de Ciencias de Materiales de Aragon, CSIC-U. de Zaragoza, Calle Pedro Cerbuna
18 12, 50009 Zaragoza, Spain

19
20

* Corresponding author: E-mail: vincent.jourdain@umontpellier.fr (V. Jourdain)

21
22

Highlights:

23
24

- One-pot, simple and fully wet method to prepare catalyst layers for the growth of VA-
25 CNT arrays.

26 - Nanotube height, diameter distribution, and crystalline quality comparable to those of
27 existing but more costly and less versatile methods.

28 - The mechanism involves the concomitant formation of an aluminum-based buffer layer
29 from aluminum hydroxides, and of catalyst nanoparticles from iron hydroxides at its
30 surface.

31
32

1 **Abstract**

2

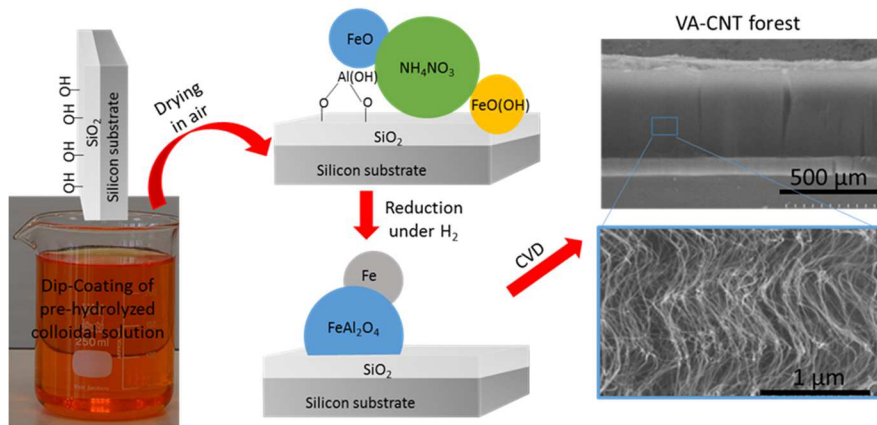
3 The catalytic growth of vertically-aligned carbon nanotubes (VA-CNTs) forest usually
4 requires thin catalyst films deposited by multi-step and costly physical vapor deposition
5 techniques. Here, we demonstrate that an efficient catalyst and its supporting layer for
6 VACNT growth can be prepared by using a simple solution of $\text{Fe}(\text{NO}_3)_3$ and $\text{Al}(\text{NO}_3)_3$
7 deposited on silica in a single step. This process being much simpler and cheaper than
8 existing preparation methods, it can easily be transferred to industry for the low-cost, thin and
9 large-area coating of catalyst for VA-CNT growth. Our study shows that aluminum
10 hydroxides preferentially react with the SiO_2 surface while iron hydroxides tend to form oxide
11 or hydroxide nanoparticles, thus allowing preparation of an aluminum-based buffer layer with
12 iron-based nanoparticles at its surface. Optimization of the Fe/Al ratio and salt concentrations
13 yielded catalysts with performances similar to standard $\text{Fe}/\text{Al}_2\text{O}_3$ catalysts prepared by
14 physical vapor deposition.

15

16

17

Graphical Abstract



18

19

20

A simple and inexpensive route of large-scale elaboration of VA-CNTs

1 1. Introduction

2
3 During the last 25 years, carbon nanotubes (CNTs) have raised a great interest due to their
4 unique structural and physical properties. Vertically aligned CNTs (VA-CNTs) arrays in
5 particular have shown great potential for many applications such as field emission [1, 2],
6 energy storage [3, 4], gas sensors [5, 6], membranes [7, 8], structural composites [9, 10] or
7 thermal interface [11, 12]. Methods to produce tall and high-quality arrays of VA-CNTs are
8 now well established, especially using the water-assisted catalytic chemical vapor deposition
9 (C-CVD) process, the so-called “super-growth” [13]. Industrial manufacturing of VA-CNTs
10 is on the rise but their production costs remain high, which strongly hinders the
11 commercialization and wide application of VA-CNT-based materials.

12 The growth process of VA-CNTs typically involves a carbon feedstock decomposed at
13 high temperature on metal catalyst nanoparticles supported on an oxide layer, such as SiO₂
14 [14], MgO [15], or Al₂O₃ [13, 16], which acts as a buffer layer to prevent catalyst ripening
15 and diffusion in the bulk of the support (usually a silicon wafer). To date, the best and
16 standard catalyst system for growing dense and tall VA-CNTs is a thin Fe film (0.4-2 nm)
17 supported on an Al₂O₃ underlayer (10-100 nm) [17]. Al₂O₃ is particularly efficient as its role
18 is not limited to a simple diffusion barrier but is also believed to reduce hydrocarbon
19 contamination of the surface in the presence of H₂O [18] and to stabilize the oxidation state of
20 iron nanoparticles (Fe²⁺ and Fe³⁺) [19], restricting iron mobility on the surface, and therefore
21 nanoparticle sintering [20]. In most studies to date on VA-CNT growth, the buffer and
22 catalyst layers are typically prepared by physical vapor deposition (PVD) [21]. Although
23 PVD systems are widely used in the semiconductor industry, a less expensive and demanding
24 process of catalyst deposition would be highly beneficial for the large-scale and continuous
25 production of VA-CNT arrays [22]. Our work was therefore motivated by the need for a
26 simpler and cheaper method of catalyst preparation for the large-scale industrial production of
27 VA-CNTs. Methods of wet deposition of metal (Fe, Co, Ni,...) have already been reported on
28 alumina or silica have been developed using metal salt solutions or metal colloid suspensions
29 as starting materials. The as-made catalysts showed activities comparable to those of PVD-
30 prepared catalysts [22-26]. Wet-deposition methods were also developed to prepare the Al₂O₃
31 underlayer [27-29]. For example, Wang *et al.* developed a fully wet procedure using boehmite
32 nanoplates (γ -AlO(OH)) deposited on a silicon chip, which were converted in a 20-nm thick
33 Al₂O₃ buffer layer by annealing at 750 °C in air. After deposition of a colloidal suspension of
34 Fe₃O₄ nanoparticles, they obtained a catalyst yielding millimeter-thick VA-CNT arrays [30].

1 However, this approach remains complex and requires several steps: i) preparation and
2 purification of the boehmite solution, ii) deposition of the particles, iii) annealing to form an
3 Al₂O₃ layer, iv) preparation and deposition of the Fe₂O₃ colloidal suspension. Our goal was
4 therefore to build on the versatility of wet methods while developing a simpler and cheaper
5 process than those previously reported.

6 Here, we report a simple and fully wet approach to prepare catalysts able to grow dense and
7 tall VA-CNT arrays on oxidized silicon wafers. The main novelty is that the aluminum-based
8 buffer layer and the catalyst nanoparticles at its surface are formed together in a single step.
9 This method is based on the dip-coating of a single solution of a mixture of Fe(NO₃)₃,
10 Al(NO₃)₃ and NH₄OH which are widely available and low-cost precursors. Although similar
11 approaches were already tested in previous works, they did not yield tall VA-CNT arrays (<
12 50 μm) [31-33]. We show here that a careful optimization of the concentrations of the
13 different species in the solution leads to a growth activity and a VA-CNT quality comparable
14 to those obtained with typical PVD-made catalysts in the same growth conditions.

16 2. Experimental

18 2.1. Materials

19 Fe(NO₃)₃·9H₂O (ACS Reagent, >98%), Al(NO₃)₃·9H₂O (ACS Reagent, >98%), NH₄OH (5
20 M) were purchased from Sigma-Aldrich and used without further purification. He (99.995%),
21 H₂ (99.9995%) and C₂H₄ (99.95%) were purchased from Linde Gas. Gas flow were controlled
22 using Brooks GF80 mass flow controllers. Silicon wafers were thermally oxidized on both
23 sides to reach a layer of 600 nm of SiO₂. For reference, PVD Al₂O₃ sublayers were prepared
24 by depositing 20 nm of Al₂O₃ by radio-frequency non-reactive sputtering. For control
25 experiments with PVD Fe, 1 nm of Fe was further evaporated on top of the Al₂O₃ layer. Just
26 prior to dip-coating, thermally oxidized Si substrates (*ca.* 15x50 mm²) were washed by
27 immersion into an active NH₄OH (5 M) / H₂O₂ (5 M) / H₂O mixture for 15 min and then
28 thoroughly washed with H₂O. Substrates coated with Al₂O₃ were thoroughly washed with
29 acetone, isopropanol and H₂O.

31 2.2. Solution and catalyst preparation

1 0.50 g of $\text{Fe}(\text{NO}_3)_3 \cdot 9\text{H}_2\text{O}$ was added to a 100 mL solution of 0.025 M NH_4OH to yield a clear
2 brown solution (Fe solution, Figure 1). Then, 0.46 g $\text{Al}(\text{NO}_3)_3 \cdot 9\text{H}_2\text{O}$ was added to yield a
3 transparent brown and acidic solution (pH \sim 4) hereafter called FeAl[X] solution with X being
4 the Fe/Al molar ratio in the solution. These solutions were then dip-coated at $20 \text{ mm} \cdot \text{min}^{-1}$ in
5 a humidity- and temperature-controlled chamber ($\text{RH} \approx 50\%$ at $27 \text{ }^\circ\text{C}$) on freshly cleaned
6 thermally oxidized silicon wafers. The samples were dried at room temperature for 1-24 h
7 before CVD experiments.

9 2.3. VA-CNT growth

11 VA-CNT growth was performed using a standard water-assisted protocol [13]. Briefly, the
12 samples were placed on top of a silicon sample holder ($40 \times 50 \text{ mm}^2$) in a 2-inches tubular
13 furnace and heated in a He/ H_2 mixture (600/400 sccm) during 15 min from room temperature
14 to $750 \text{ }^\circ\text{C}$. At $750 \text{ }^\circ\text{C}$, 200 ppm of H_2O were added using a small flow of He in a water
15 bubbler which was maintained at low temperature (typically $5 \text{ }^\circ\text{C}$) and the samples were kept
16 at $750 \text{ }^\circ\text{C}$ in this atmosphere for 5 min. Humidity was controlled using an hygrometer (MIS
17 Probe 2, General Electrics) prior to each experiment. Then, the samples were exposed for 10
18 min to a He/ C_2H_4 mixture (810/190 sccm) with 200 ppm H_2O to grow VA-CNTs. The furnace
19 was then cooled under He at a temperature below $100 \text{ }^\circ\text{C}$ before opening and withdrawal of
20 the samples to prevent VACNT oxidation.

21 The samples presented in this study were prepared in four different runs. During each run, a
22 reference catalyst prepared by PVD with 1 nm of Fe on 20 nm of Al_2O_3 (PVD: Fe@ Al_2O_3)
23 was added in the furnace and the thickness of VACNT grown on it was controlled by an
24 optical camera to confirm the reproducibility of the growth conditions independently of the
25 environmental conditions.

27 2.4. Characterization

29 Scanning electron micrographs were obtained using a Hitachi S4800 operating at 10 kV.
30 Raman characterization of the VA-CNTs was performed at a laser wavelength of 532 nm
31 using a Horiba Jobin-Yvon T64000 spectrometer equipped with a silicon camera cooled with
32 liquid nitrogen and a microscope. The focused laser spot on the sample was typically $1 \text{ } \mu\text{m}$.
33 Atomic force micrographs were obtained using a Bruker AFM D3100 in tapping mode using
34 a NCH point probe with a tip radius of 5 nm at $F = 242.9 \text{ kHz}$, $Q = 460$ and $k = 18 \text{ N} \cdot \text{m}^{-1}$. X-

1 Ray Photoelectron spectroscopy (XPS) measurements were performed on Mepitel®. The
2 excitation source produced a monochromatic Al K α line (1486.6 eV) and worked at 100 W of
3 power. The analyzed surface had a 400- μ m diameter. All XPS components were assigned
4 from the analysis of the values reported for reference compounds and referenced in the NIST
5 database [34]. X-Ray diffraction (XRD) patterns were obtained using a PAN analytical X'Pert
6 Pro MPD diffractometer at Cu K α irradiation ($\lambda = 1.5418 \text{ \AA}$) with a step size of 0.033° (2θ
7 scale) in the $12^\circ - 80^\circ$ interval. Note that in the case of powders submitted to a reducing
8 treatment for subsequent XRD characterization, the samples were stored under inert gas just
9 after the reducing treatment to prevent oxidation in air. For other samples, they were normally
10 exposed to air as during the elaboration process before XRD and oxidation in air was taken
11 into account for the XRD interpretation. Transmission Electron Microscopy (TEM) was first
12 performed on a JEOL 1200 EX II operated at 100 kV. High-Resolution TEM (HRTEM)
13 micrographs were obtained with a FEI Titan Cs image aberration-corrected microscope
14 working at 80 kV. In the latter case, the observations were performed at low temperature
15 (approx. 77 K) to avoid electron irradiation damage of the nanotubes and possible
16 contamination of the samples. Micrographs were subsequently analyzed using the Gatan
17 Digital Micrograph software taking intensity profiles through each tube to measure their
18 diameter distribution.

19

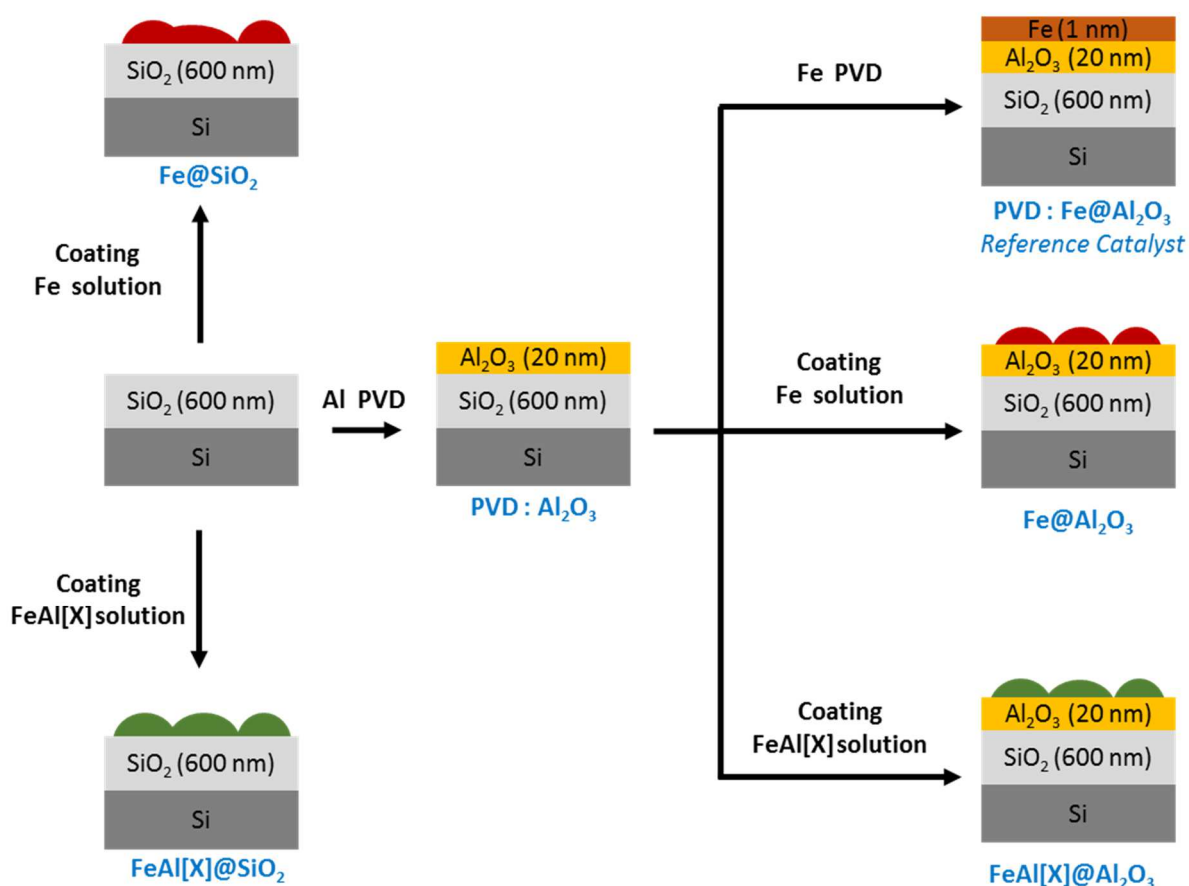
20 3. Results

21

22 We first studied the influence of the catalyst preparation parameters on the features of the
23 grown CNTs. Figure 1 shows the typical procedure for the experiments conducted throughout
24 this study. First, we investigated the activity of a solution of Fe(NO $_3$) $_3$ in dilute NH $_4$ OH (Fe
25 solution). The role of NH $_4$ OH is to allow the formation of metal hydroxides able to condense
26 into nanoparticles. This solution was dip-coated on a thermally oxidized Si wafer (Fe@SiO $_2$)
27 and on a silicon wafer coated with an extra layer of 20 nm of Al $_2$ O $_3$ deposited by PVD
28 (Fe@Al $_2$ O $_3$). The activity of these catalysts was compared to that of a reference catalyst
29 prepared by PVD with 1 nm of Fe on 20 nm of Al $_2$ O $_3$ (PVD: Fe@Al $_2$ O $_3$). In each run, the
30 thickness of the VA-CNTs grown on the reference PVD catalyst was measured to be 660 μ m
31 +/- 10 %, thus confirming the good reproducibility of the growth conditions. We observed
32 that thick VA-CNT arrays were grown on both PVD:Fe@Al $_2$ O $_3$ and Fe@Al $_2$ O $_3$, with
33 thickness of, respectively, 650 μ m and 590 μ m (Table 1, entries 1 and 2). At the opposite, a
34 thin layer of entangled CNTs was grown with Fe@SiO $_2$, in good agreement with previous

1 studies performed in the absence of an alumina under-layer [35, 36]. Second, we studied the
 2 influence of a PVD Al_2O_3 under-layer on the activity of the $\text{FeAl}[X]$ catalysts. As shown in
 3 table 1 (entry 3), a $\text{FeAl}[1]$ solution dip-coated on PVD Al_2O_3 ($\text{FeAl}[1]@\text{Al}_2\text{O}_3$) yielded a
 4 VA-CNT array with a thickness of $690\ \mu\text{m}$, while a slightly thinner array ($550\ \mu\text{m}$) was
 5 obtained with the same solution deposited on Si/SiO_2 ($\text{FeAl}[1]@\text{SiO}_2$, entry 7). Together,
 6 these results confirm the well-documented effect that an Al_2O_3 under-layer strongly promotes
 7 VA-CNT growth from Fe catalyst nanoparticles.

8



9

10 **Figure 1. Protocols of catalyst preparation and corresponding catalyst nomenclature.**

11 Third, we studied the influence of the Fe/Al ratio ($X=[\text{Fe}]/[\text{Al}]$) on the activity of the
 12 $\text{FeAl}[X]@\text{Al}_2\text{O}_3$ catalysts. The maximum VA-CNT thickness ($660\ \mu\text{m}$) was obtained with a
 13 Fe/Al ratio of 0.6 ($\text{FeAl}[0.6]@\text{SiO}_2$, Table 1, entry 5). Importantly, this thickness is
 14 comparable to the one obtained with the reference PVD catalyst thus demonstrating that
 15 catalysts prepared by a simple dip-coating step can yield VA-CNT forests with heights similar
 16 to PVD-made catalysts. Higher and lower Fe/Al ratio yielded thinner VA-CNT layers (Table
 17 1, entries 4-9).

1 Fourth, the effect of increasing the total concentration of Fe and Al salts was investigated. By
 2 doubling the total concentration in Fe and Al salts, significantly taller VA-CNTs were
 3 obtained: 640 μm for **2xFeAl[1]@SiO₂** (entry 12) by comparison to 550 μm for
 4 **FeAl[1]@SiO₂** (entry 7). Note that for Fe solution deposited on PVD Al₂O₃, doubling the Fe
 5 concentration has little effect: 620 μm for **2xFe@Al₂O₃** (entry 10) to be compared to 590 μm
 6 for **Fe@Al₂O₃** (entry 2). All together, these results highlight the high potential of this fully-
 7 wet single-step approach since a simple coating by Fe and Al salt solutions directly on
 8 Si/SiO₂ shows performances comparable to those of PVD catalysts.

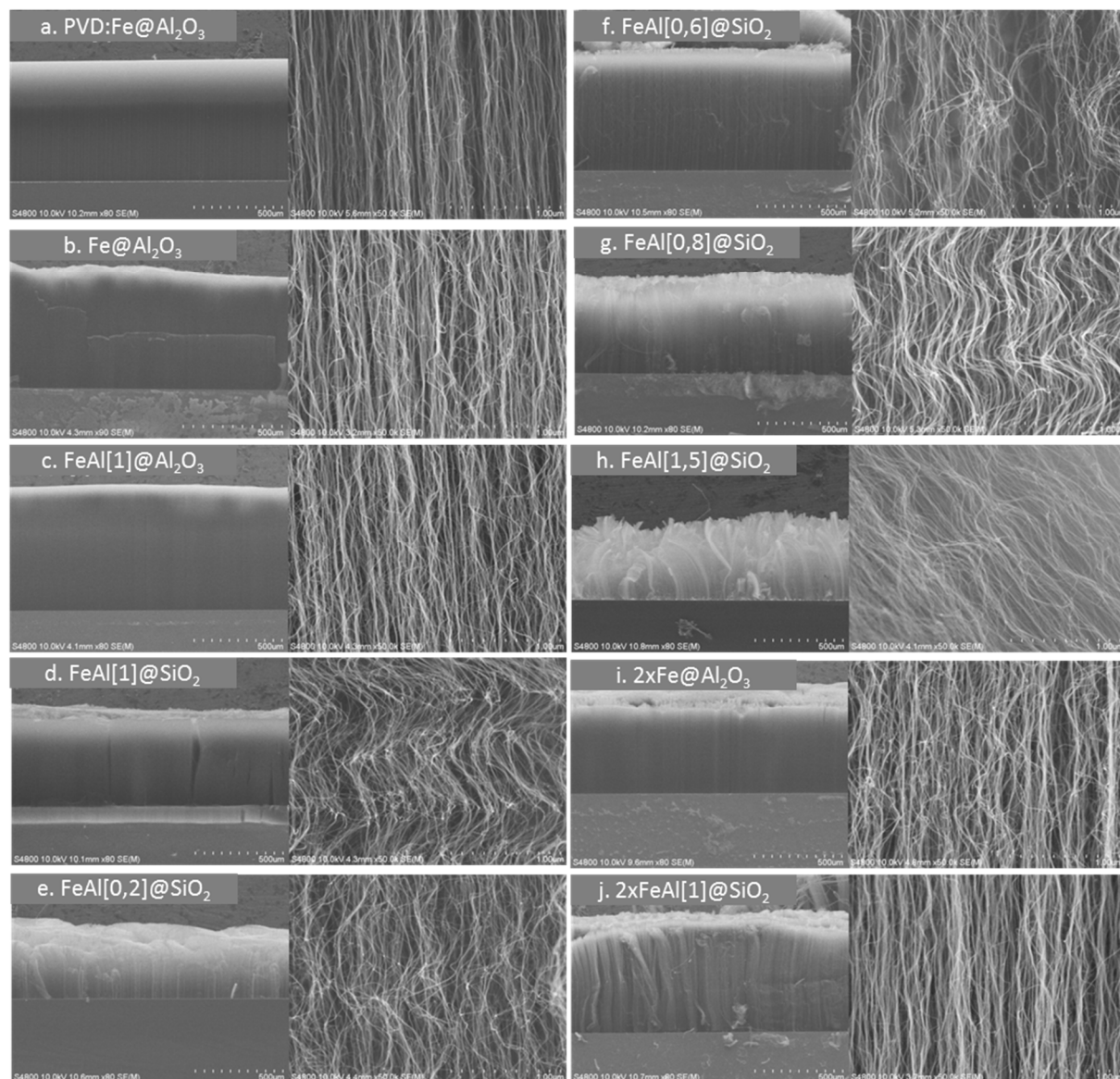
9 The morphologies of the VA-CNT arrays were then analyzed by scanning electron
 10 microscopy (SEM) as shown in Figure 2. SEM pictures showed well aligned CNTs on all the
 11 samples grown on Al₂O₃ (Fig. 2a-c) while less aligned and curly CNTs were observed for the
 12 samples grown from **FeAl[X]@SiO₂** (Fig. 2d-h) with X between 0.2 and 1.5. Since alignment
 13 is essentially caused by steric interactions between CNTs, this supports that **FeAl[X]@SiO₂**
 14 **catalysts yield** a lower CNT density of the VACNT forests than PVD catalysts. In general, a
 15 lower homogeneity in CNT height was observed in VA-CNTs grown from **FeAl[X]@SiO₂**
 16 catalysts when compared to PVD catalysts, which also points toward a less homogeneous and
 17 less dense distribution of active catalyst particles.

18
 19 **Table 1. VA-CNT height, Raman G-band positions and G/D ratio ($\lambda = 532 \text{ nm}$) of the**
 20 **samples grown from the different catalysts.**

Entry	Catalyst	[Fe] (mol.L ⁻¹)	[Fe]/[Al]	VA-CNT height (μm)	G band (cm ⁻¹)	G/D ratio
1	PVD: Fe@Al₂O₃	N/A	N/A	660 +/- 10%	1584	3.2
2	Fe@Al₂O₃	0.0125	N/A	590	1583	2.2
3	FeAl[1]@Al₂O₃	0.0125	1	690	1581	3.7
4	FeAl[0.2]@SiO₂	0.0125	0.2	420	1576	1.1
5	FeAl[0.6]@SiO₂	0.0125	0.6	660	1576	1.2
6	FeAl[0.8]@SiO₂	0.0125	0.8	550	1578	2.8
7	FeAl[1]@SiO₂	0.0125	1	550	1579	1.5
8	FeAl[1.5]@SiO₂	0.0125	1.5	450	1584	1.5
9	FeAl[2]@SiO₂	0.0125	2	250	1577	1.2

10	$2xFe@Al_2O_3$	0.25	N/A	620	1575	4.8
11	$2xFeAl[0.8]@SiO_2$	0.25	0.8	n.d.	1580	2.5
12	$2xFeAl[1]@SiO_2$	0.25	1	640	1580	3.1

1

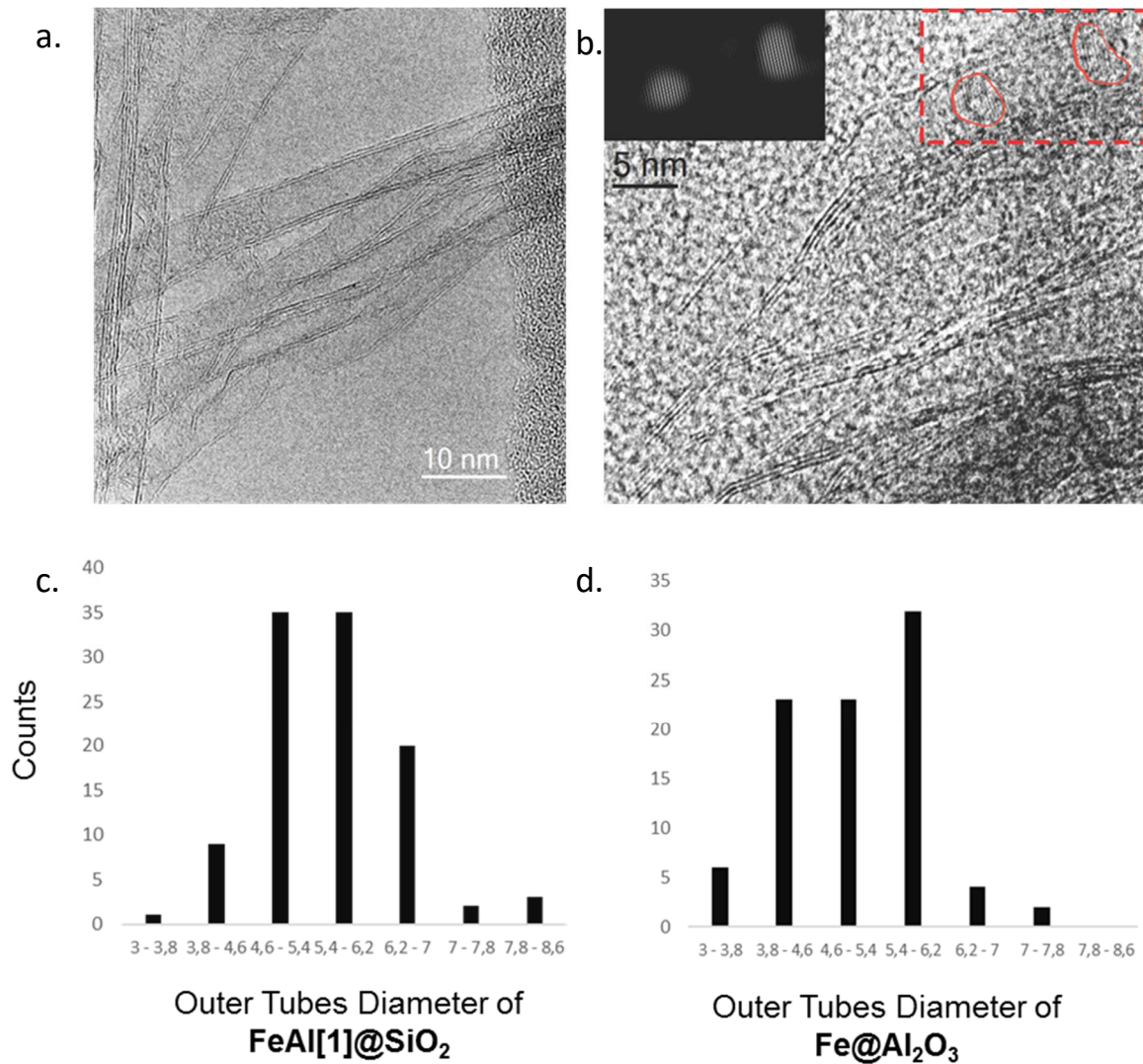


2

3

4 **Figure 2. SEM pictures of the VA-CNTs grown from: a. PVD: Fe@Al₂O₃, b. Fe@Al₂O₃,**
5 **c. FeAl[1]@Al₂O₃, d. FeAl[1]@SiO₂, e. FeAl[0.2]@SiO₂, f. FeAl[0.6]@SiO₂, g.**
6 **FeAl[0.8]@SiO₂, h. FeAl[1.5]@SiO₂, i. 2xFe@ Al₂O₃, j. 2xFeAl[1]@SiO₂.**

7

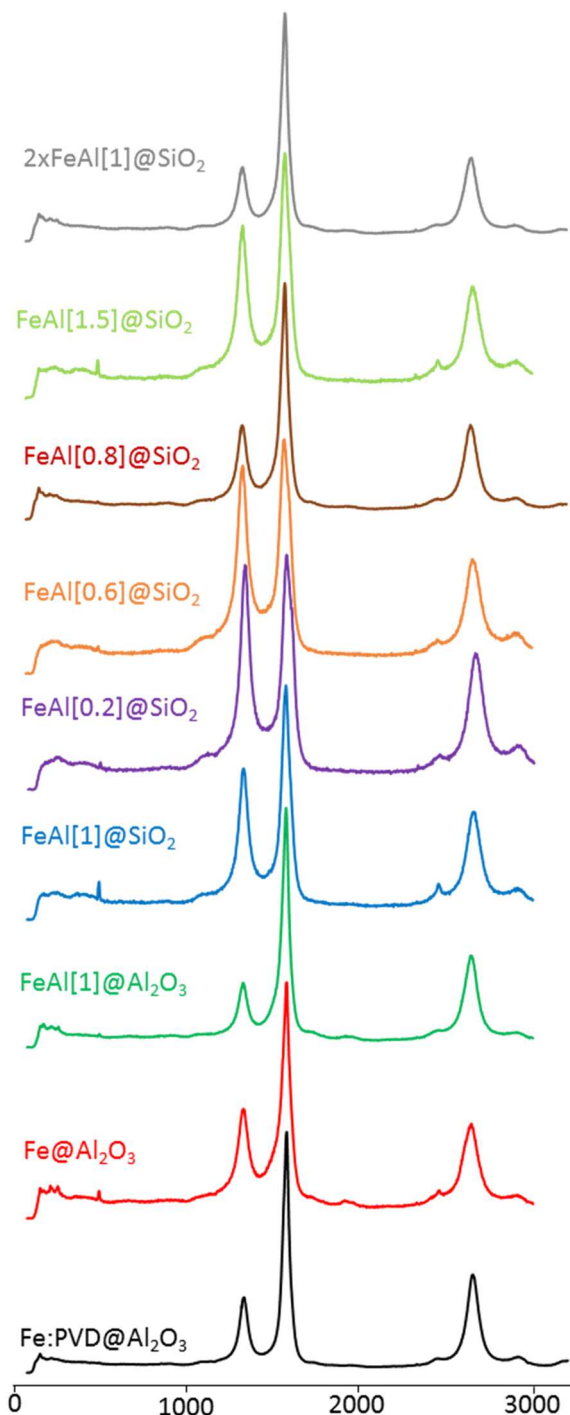


1

2 **Figure 3. a,b) Representative HRTEM pictures of CNTs and catalyst crystalline**
 3 **nanoparticles (highlighted by a red contour) after growth using the FeAl[1]@SiO₂**
 4 **catalyst. In b), a Fast Fourier Transform (FFT) has been applied to the TEM image and**
 5 **the crystalline spots corresponding to the catalyst NPs have been selected to apply an**
 6 **inverse FFT for building the insert image at the top left. c,d) Outer tubes diameter**
 7 **distribution diagram of FeAl[1]@SiO₂ (c) and Fe@Al₂O₃ (d), respectively.**

8 The diameter distribution of the CNTs grown from **PVD: Fe@Al₂O₃**, **Fe@Al₂O₃**, and
 9 **FeAl[1]@SiO₂** were evaluated by TEM and found to be comparable for the three samples
 10 with most tubes having diameters of 5 +/- 1 nm. The structure of the CNTs grown from
 11 **FeAl[1]@SiO₂** was further analyzed by high-resolution TEM showing that mainly double-
 12 and triple-wall CNTs were obtained (Figure 3, mean size 5.6 +/- 1.6 nm with a ratio of 2.4
 13 DWCNTs for 1 TWCNT). By comparison, VA-CNTs grown from **Fe@Al₂O₃** showed slightly
 14 thinner nanotubes with a higher proportion of DWCNTs (5.2 +/- 0.8 nm with 3.3 DWCNTs

1 for 1 TWCNT, Figure 3). The crystalline quality of all CNTs was found relatively good and
2 comparable to that reported in the literature for VA-CNTs grown from PVD-made catalysts.



3

4 **Figure 4. Raman spectra of VA-CNT arrays grown from the different catalysts.**

5

6 The samples were then analyzed by micro-Raman spectroscopy (Figure 4). All the VA-CNTs
7 samples showed a G band at around 1580 cm⁻¹ (see Table 1) as expected from a sample

1 dominated by multi-walled CNTs (MWCNTs) with diameters in the range of 3-7 nm as
2 measured by HRTEM (Figure 3). All samples also displayed D and 2D (G') bands at
3 positions in the range of 1327-1338 cm^{-1} and 2642-2670 cm^{-1} , respectively. This is also in
4 good agreement with the positions expected for MWCNTs at 532 nm of laser excitation.
5 Many samples showed additional signals at low frequencies (less than 280 cm^{-1}) associated
6 with the radial breathing modes (RBMs) of small diameter CNTs ($d = 1-3$ nm). The
7 occurrence of RBMs is systematically associated with higher intensities of the G and 2D
8 bands and to downshifted D and 2D bands as also expected when moving toward such
9 smaller-diameter CNTs. Since CNTs of 1-3 nm were not observed during our HRTEM
10 observations but display an intrinsically higher Raman cross section due to the resonance
11 effect, the results agree with samples mainly composed of double/triple-wall CNTs with 3-7
12 nm diameter with traces of CNTs with 1-3 nm diameter. The proportion of small-diameter
13 CNTs was generally found higher for the catalysts deposited on PVD alumina. Note that
14 having a mixture of large-diameter CNTs (weakly resonant and with low G/D ratio) and
15 small-diameter CNT (highly resonant and with high G/D ratio) hinders the use of the G/D
16 ratio (Table 1) to evaluate the overall crystalline purity of the sample. Instead, for the samples
17 studied here, a higher G/D ratio essentially denotes a higher proportion of small-diameter
18 CNTs in agreement with the other Raman features (more intense RBMs, downshifted D and
19 2D bands). By comparing the Raman spectra at different positions, one may roughly estimate
20 that large- and small-diameter CNTs display a G/D ratio in the range of 1-2 and 2-6,
21 respectively and quite independently of the catalyst. Of course, this value is expected to
22 strongly vary with the growth conditions (temperature, precursor pressure) used [37]. Overall,
23 the TEM and Raman results shows that our wet-based catalyst preparation method allows the
24 preparation of VA-CNT arrays with similar morphology and structural quality than standard
25 PVD catalyst, yet with the use of simpler protocol and laboratory equipment.

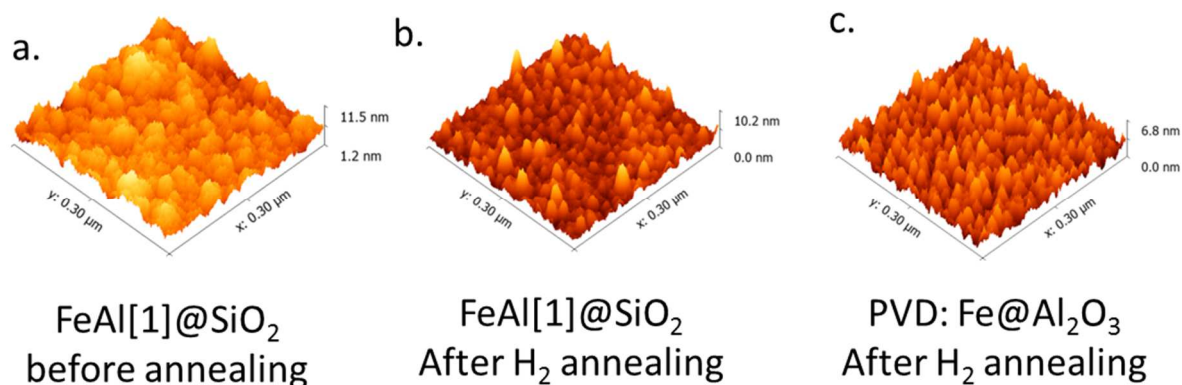
26

27 **4. Discussion**

28

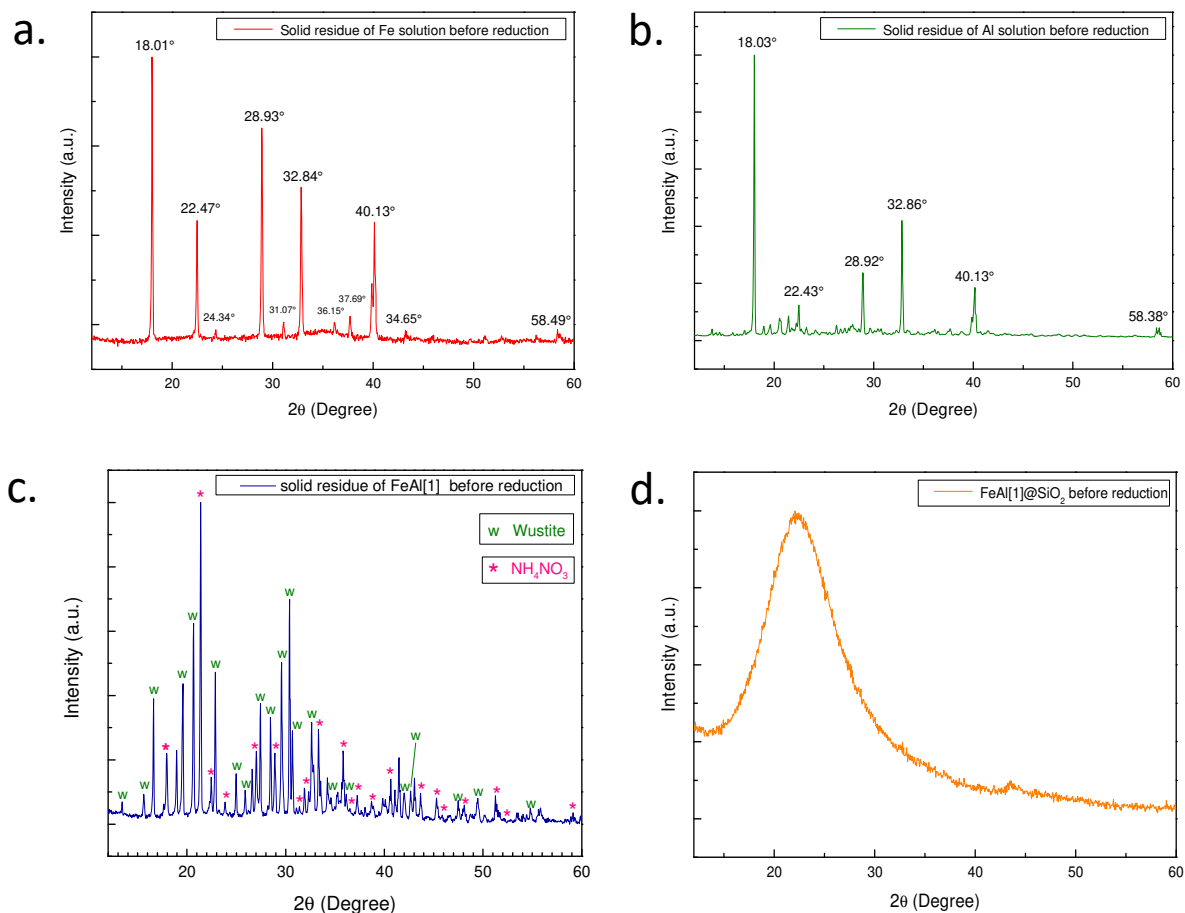
29 To understand the effect of the addition of the Al salt, the catalyst formation mechanism was
30 investigated using Atomic Force Microscopy (AFM), X-ray Diffraction (XRD) and X-ray
31 Photoelectron Spectroscopy (XPS).

32



1
 2 **Figure 5.** AFM images of a. FeAl[1]@SiO₂ before annealing, b. FeAl[1]@SiO₂ after
 3 annealing at 750 °C under H₂ and c. PVD: Fe@Al₂O₃ after annealing at 750 °C under
 4 H₂.

5
 6 AFM observations of the samples after deposition of solution FeAl[1] on Si/SiO₂ and drying
 7 were first performed. As shown in Figure 5a, large nanoparticle aggregates of 10-50 nm were
 8 observed on the surface. Since the diameter of a MWCNT is strongly related to the size of its
 9 catalyst particle [36, 38], these particles are not likely to be directly responsible for the
 10 observed catalytic activity since the CNT diameter distribution was determined to be 5.6 +/-
 11 1.6 nm (Figure 3c). Interestingly, after annealing at 750°C under a He/H₂ mixture with 200
 12 ppm H₂O and rapid cooling to RT under a He/H₂ flow, well-defined and smaller nanoparticles
 13 were observed (height around 5 nm) on the surface (Figure 5b). When compared to the PVD
 14 catalyst (Figure 5c) whose surface is very homogeneous after reduction, FeAl[1]@SiO₂
 15 surface shows the presence of some larger nanoparticles (around 10 nm in height). This is in
 16 good agreement with our SEM observations of less dense and curly VA-CNTs [39] obtained
 17 with the catalysts prepared by dip-coating. From AFM measurements, it is clear that a severe
 18 surface reconstruction occurs during the H₂ treatment.



1
2 **Figure 6. a. XRD of the dry residue of $\text{Fe}(\text{NO}_3)_3$ aqueous solution with 1 equivalent of**
3 **NH_4OH before reduction showing mainly the presence of NH_4NO_3 [40] (ICSD collection**
4 **code 002772). b. XRD of the dry residue of a $\text{Al}(\text{NO}_3)_3$ aqueous solution with 1**
5 **equivalent of NH_4OH before reduction showing mainly the presence of NH_4NO_3 [40] c.**
6 **XRD of a dry residue of a $\text{FeAl}[1]$ solution showing mainly the presence of Wuestite**
7 **(Iron Oxide $\text{Fe}_{0.902}\text{O}$) [41] (ICSD collection code 040089) and NH_4NO_3 [40]. d. XRD of**
8 **$\text{FeAl}[1]$ impregnated on high surface area silica solution after reduction under H_2 at**
9 **750°C showing only the typical large shoulder of amorphous silica.**

10 To further investigate the composition of the thin catalyst film before CVD experiments,
11 XRD measurements of the solid residue obtained after evaporation of the different solutions
12 were performed. Before reduction, the solid residue of a $\text{Fe}(\text{NO}_3)_3$ aqueous solution with 1
13 equivalent of NH_4OH (Fe solution) showed the presence of crystalline NH_4NO_3 (Figure 6a)
14 with average crystal sizes larger than 100 nm. The same result was obtained for the solid
15 residue of a $\text{Al}(\text{NO}_3)_3$ aqueous solution with 1 equivalent of NH_4OH (Figure 6b). The residue
16 of $\text{FeAl}[1]$ also showed the presence of crystalline NH_4NO_3 nanoparticles, along with
17 crystalline FeO nanoparticles (Figure 6c). However, there was no signature of crystalline Al-

1 based compounds. Interestingly, when solution **FeAl[1]** was coated on high surface-area silica
 2 and reduced under H₂, no diffraction peaks were observed, which indicates that large metallic
 3 Fe nanoparticles were not formed in agreement with AFM observations (Figure 6d). The
 4 disappearance of the large NH₄NO₃ crystal nanoparticles previously observed provides an
 5 explanation for the evolution of surface roughness observed by AFM before and after H₂
 6 reduction as further supported by the decomposition temperature of NH₄NO₃ (210°C).

7
 8 XPS analysis were then performed. Surface analysis of sample **FeAl[1]@SiO₂** after drying,
 9 but before reduction under H₂, showed a very large contribution of the SiO₂ substrate with
 10 25.5% of Si, and only 5.0% of Al and 5.0% of Fe (Table 2).

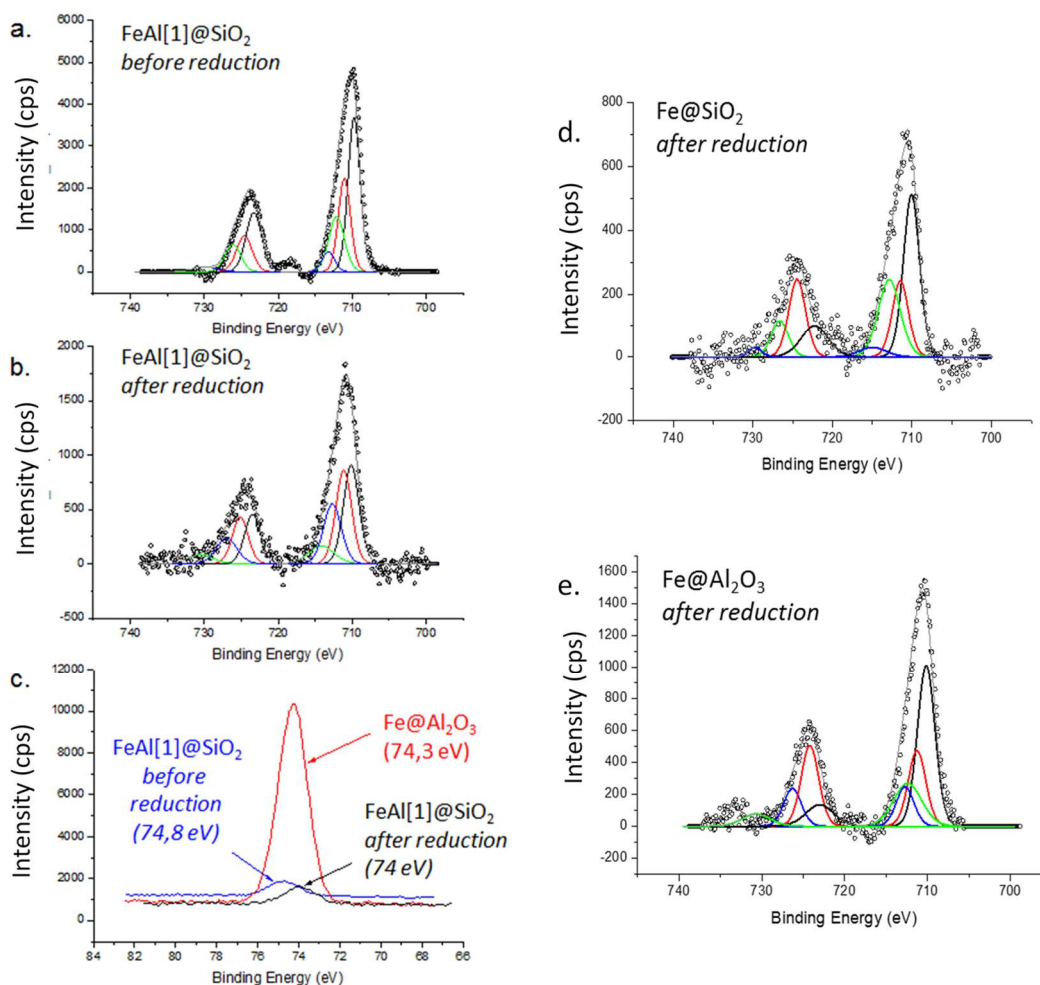
11
 12 **Table 2. Surface composition of the catalyst: elemental composition from XPS.**

Sample Name	Treatment	Si (2p)	O (1s)	Fe (2p)	Al (2p)
FeAl[1]@SiO₂	after deposition	25.7	64.2	5.1	5.1
FeAl[1]@SiO₂	after H ₂ reduction	36.7	58.3	1.2	3.7
Fe@SiO₂	after H ₂ reduction	41.1	58.4	0.5	0,0
Fe@Al₂O₃	after H ₂ reduction	0,0	55.8	1.0	43.1

13
 14 Since XPS is only sensitive to the top 10 nm of the surface, this indicates that the deposited
 15 layer is very thin (less than 10 nm) and/or not continuous. The Fe 2p_{3/2} profile is made of two
 16 contributions: an Fe(II) contribution at 709.8 eV and an Fe(III) contribution at 711.1 eV with
 17 a Fe(II)/Fe(III) ratio of 1.65, plus two satellite peaks at higher energy (Figure 7a) . This
 18 excludes the presence of metallic iron (expected at ~707 eV), of iron silicide (Fe₃Si expected
 19 at 707.5 eV) and of iron silicate (Fe₂SiO₄ expected at 708.9-709.0 eV). It also excludes the
 20 possibility of a single Fe(II) or Fe(III) compound, or of Fe₃O₄ only (which has an
 21 Fe(II)/Fe(III) ratio of 0.5). For the Fe(III) peak at 711.1 eV, the most likely assignment is
 22 FeO(OH) (expected at 711.0-711.8 eV) or alternatively Fe₂O₃ (which is expected at 710.7-
 23 711.4 eV). For the Fe(II) peak at 709.8 eV, the most likely assignment is FeO which is
 24 expected at 709.6-710.3 eV. The Al 2p peak is found at 74.8 eV (Figure 7c) which would
 25 nicely agree with an aluminosilicate such as Al₂OSiO₄ (expected at 74.5-74.9 eV) or an
 26 aluminum silicate hydroxide such as Al₂Si₄O₁₀(OH)₂ (expected at ~74.7 eV), which in both
 27 cases would support a strong anchoring of aluminum with the SiO₂ substrate.

1 After H₂ annealing, an even larger atomic contribution of Si (36.6 %) was observed, with
2 3.7% of Al and 1.2% of Fe remaining on the surface (Table 2), showing significant Fe
3 diffusion in the SiO₂ matrix at high temperature (750°C). The Fe 2p_{3/2} profile displayed little
4 change with still two contributions: an Fe(II) contribution at 710.1 eV and an Fe(III)
5 contribution at 711.4 eV with about the same Fe(II)/Fe(III) ratio as before reduction (Figure
6 7b). At the opposite, the Al 2p peak was strongly downshifted to 74.0 eV (Figure 7c), which
7 could be assigned to Al(OH)₃ (expected at 73.9-74.4 eV) or alternatively to FeAl₂O₄
8 (expected at ~74.3 eV). The latter one should give rise to an Fe 2p_{3/2} contribution at ~710.0
9 eV which is in good agreement with the Fe(II) peak observed at 710.1 eV. We performed the
10 same H₂ treatment and XPS analysis on the same solution without Al(NO₄)₃ (*i.e.* Fe@SiO₂)
11 and found that the amount of Fe remaining at the surface was about three times less (Table 2).
12 This provides an additional support for the formation of an iron aluminate such as FeAl₂O₄
13 which would stabilize Fe at the surface of SiO₂. The remaining Fe(III) peak is assigned to
14 Fe₂O₃ and/or FeO(OH) formed from reduced iron when exposed to air (Figure 7d).
15

1



2

3

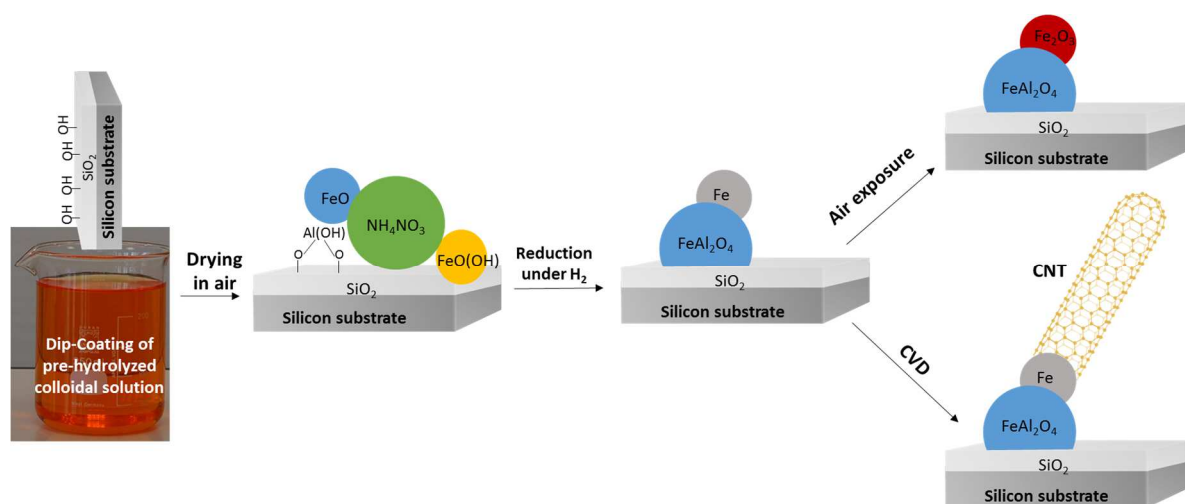
4 **Figure 7. Fe 2p XPS spectra of a) FeAl[1]@SiO₂ before H₂ reduction, and b) after H₂**
5 **reduction; c) Al 2p XPS spectra of FeAl[1]@SiO₂ before H₂ reduction (blue), and after**
6 **H₂ reduction (black) compared to Fe@Al₂O₃ after H₂ reduction (red); Fe 2p XPS**
7 **spectra of d) Fe@SiO₂ after H₂ reduction and e) Fe@Al₂O₃ after H₂ reduction.**

8

9 Taken together, these results support the following picture (Figure 8). During air drying,
10 Al(OH)₃ tends to react with the SiO₂ surface (e.g. with hydroxyl groups) to form a surface
11 layer of aluminosilicate or aluminum silicate hydroxide compounds, while Fe(OH)₃ tends to
12 form FeO or FeO(OH) nanoparticles. During H₂ annealing, particles of Fe oxides and
13 hydroxides can either get reduced to metallic iron which then tends to diffuse into the SiO₂
14 substrate. Alternatively, in the presence of surface aluminum oxides or hydroxides, they can
15 form surface layers of iron aluminates which are less reducible and act as a buffer layer which
16 stabilizes small iron nanoparticles at their surface. So, beside its standard role of diffusion

1 barrier, SiO_2 plays another role in our process, by allowing the formation of a mixed Al-Si
 2 oxidized layer which will anchor and stabilize catalyst nanoparticles. If exposed to a carbon
 3 source during CVD, these stabilized iron particles will allow the growth of long CNTs.
 4 Instead, if exposed to air, these iron nanoparticles will quickly become oxidized into Fe(III)
 5 compounds such as Fe_2O_3 or $\text{FeO}(\text{OH})$. This mechanism supports that increasing the
 6 concentration of Al in the solution at constant ratio with Fe should increase the surface
 7 coverage with aluminum compounds and therefore a higher density of stabilized iron particles
 8 and so a higher yield of long and defective nanotubes: this is in perfect line with our previous
 9 observation that doubling the proportion of Fe and Al promotes both a taller VACNT forest
 10 and a lower defect density (see entry 12 of table 1).

11



12

13 **Figure 8.** Proposed mechanism for catalyst formation and evolution.

14

15 5. Conclusion

16

17 In this study, a fully wet process was developed to prepare, in a single deposition step, a
 18 catalyst to grow VA-CNT arrays on standard SiO_2/Si wafers. This is important from a
 19 materials engineering point of view because the process is much simpler and cheaper than
 20 existing preparation methods. We therefore expect it to be easily transferred to industry for
 21 low-cost and large-area coating of catalyst for VA-CNT growth. This catalyst, prepared from
 22 a mixture of $\text{Fe}(\text{NO}_3)_3$ and an $\text{Al}(\text{NO}_3)_3$, yields VACNT height comparable to those of
 23 $\text{Fe}/\text{Al}_2\text{O}_3$ catalysts prepared by PVD which is standardly used for VA-CNT growth. Our study
 24 showed that, when mixed together, aluminum hydroxides preferentially react with the SiO_2

1 surface while iron hydroxides tend to react together to form oxide or hydroxide nanoparticles:
2 this explains why a single solution step can be used to prepare both an aluminum-based buffer
3 layer and catalyst nanoparticles at its surface. This is important from a materials science point
4 of view because it shows that chemical affinities between reactants can be played with to
5 elaborate the catalyst nanoparticles and their supporting layer together in a single step.
6 Following this initial demonstration, the approach may be further optimized and generalized
7 to other catalysts to increase the homogeneity and density of the CNT forest and obtain a
8 better control of the CNT diameter and crystalline quality. This simple and versatile approach
9 appears as a strong alternative to PVD to easily prepare VA-CNT forests on various
10 substrates, such as curved, porous or conducting substrates. Importantly for applications in
11 electronics and electrochemistry requiring to electrically contact VA-CNT arrays, this process
12 requires only a very thin layer of insulating oxide material, therefore allowing a more intimate
13 contact between CNTs and their substrate.

14

15 **Acknowledgement**

16 We thank Michel Ramonda and the Near-Field Microscopy service (CTM) of the University
17 of Montpellier for AFM analyses. HRTEM studies were conducted at the Laboratorio de
18 Microscopias Avanzadas, Instituto de Nanociencia de Aragon, Universidad de Zaragoza,
19 Spain.

20 The Government of Aragon, and the European Social Fund are gratefully acknowledged. R.A.
21 gratefully acknowledges the project “Construyendo Europa desde Aragon” 2014-2020 (grant
22 number E/26). R.A. gratefully acknowledges the support from the Spanish Ministry of
23 Economy and Competitiveness (MINECO) through project grant MAT2016-79776-P
24 (AEI/FEDER, UE). Part of this work has received funding from the European Union’s
25 Horizon 2020 research and innovation program under the Marie Skłodowska-Curie grant
26 agreement No 642742.

27

28 **Data availability**

29 No raw/processed data are required to reproduce these findings.

30

31 **References**

32

33 [1] W.A. de Heer, A. Châtelain, D. Ugarte, A Carbon Nanotube Field-Emission Electron
34 Source, *Science*. 270 (1995) 1179-1180. <https://doi.org/10.1126/science.270.5239.1179>

- 1 [2] N. Perea-López, B. Rebollo-Plata, J.A. Briones-León, A. Morelos-Gómez, D. Hernández-
2 Cruz, G.A. Hirata, V. Meunier, A.R. Botello-Méndez, J.-C. Charlier, B. Maruyama, E.
3 Muñoz-Sandoval, F. López-Urías, M. Terrones, H. Terrones, Millimeter-Long Carbon
4 Nanotubes: Outstanding Electron-Emitting Sources, *ACS Nano*. 5 (2011) 5072-5077.
5 <https://doi.org/10.1021/nn201149y>
- 6 [3] D.N. Futaba, K. Hata, T. Yamada, T. Hiraoka, Y. Hayamizu, Y. Kakudate, O. Tanaike, H.
7 Hatori, M. Yumura, S. Iijima, Shape-engineerable and highly densely packed single-
8 walled carbon nanotubes and their application as super-capacitor electrodes, *Nat Mater*. 5
9 (2006) 987-994. <https://doi.org/10.1038/nmat1782>
- 10 [4] K. Byungwoo, C. Haegeun, K. Woong, High-performance supercapacitors based on
11 vertically aligned carbon nanotubes and nonaqueous electrolytes, *Nanotechnology*. 23
12 (2012) 155401. <https://doi.org/10.1088/0957-4484/23/15/155401>
- 13 [5] Y. Wang, J.T.W. Yeow, A Review of Carbon Nanotubes-Based Gas Sensors, *Journal of*
14 *Sensors*. 2009 (2009) 24. <https://doi.org/10.1155/2009/493904>
- 15 [6] D.R. Kauffman, A. Star, Carbon Nanotube Gas and Vapor Sensors, *Angewandte Chemie*
16 *International Edition*. 47 (2008) 6550-6570. <https://doi.org/10.1002/anie.200704488>
- 17 [7] B.J. Hinds, N. Chopra, T. Rantell, R. Andrews, V. Gavalas, L.G. Bachas, Aligned
18 Multiwalled Carbon Nanotube Membranes, *Science*. 303 (2004) 62-65.
19 <https://doi.org/10.1126/science.1092048>
- 20 [8] F. Du, L. Qu, Z. Xia, L. Feng, L. Dai, Membranes of Vertically Aligned Superlong
21 Carbon Nanotubes, *Langmuir*. 27 (2011) 8437-8443. <https://doi.org/10.1021/la200995r>
- 22 [9] H. Cebeci, R.G.d. Villoria, A.J. Hart, B.L. Wardle, Multifunctional properties of high
23 volume fraction aligned carbon nanotube polymer composites with controlled
24 morphology, *Composites Science and Technology*. 69 (2009) 2649-2656.
25 <https://doi.org/10.1016/j.compscitech.2009.08.006>
- 26 [10] V.P. Veedu, A. Cao, X. Li, K. Ma, C. Soldano, S. Kar, P.M. Ajayan, M.N. Ghasemi-
27 Nejjhad, Multifunctional composites using reinforced laminae with carbon-nanotube
28 forests, *Nat Mater*. 5 (2006) 457-462. <https://doi.org/10.1038/nmat1650>
- 29 [11] T. Tong, Y. Zhao, L. Delzeit, A. Kashani, M. Meyyappan, A. Majumdar, Dense
30 vertically aligned multiwalled carbon nanotube arrays as thermal interface materials,
31 *IEEE Transactions on Components and Packaging Technologies*. 30 (2007) 92.
32 <https://doi.org/10.1109/TCAPT.2007.892079>
- 33 [12] J. Liu, T. Wang, Y. Fu, L. Ye, Use of carbon nanotubes in potential electronics
34 packaging applications, in 10th IEEE International Conference on Nanotechnology
35 (IEEE-NANO), Seoul, South Korea, IEEE, 2010, 160-166.
36 <https://doi.org/10.1109/NANO.2010.5698052>
- 37 [13] K. Hata, D.N. Futaba, K. Mizuno, T. Namai, M. Yumura, S. Iijima, Water-Assisted
38 Highly Efficient Synthesis of Impurity-Free Single-Walled Carbon Nanotubes, *Science*.
39 306 (2004) 1362-1364. <https://doi.org/10.1126/science.1104962>
- 40 [14] S. Maruyama, E. Einarsson, Y. Murakami, T. Edamura, Growth process of vertically
41 aligned single-walled carbon nanotubes, *Chemical Physics Letters*. 403 (2005) 320-323.
42 <https://doi.org/10.1016/j.cplett.2005.01.031>
- 43 [15] G.-Y. Xiong, D.Z. Wang, Z.F. Ren, Aligned millimeter-long carbon nanotube arrays
44 grown on single crystal magnesia, *Carbon*. 44 (2006) 969-973.
45 <https://doi.org/10.1016/j.carbon.2005.10.015>
- 46 [16] S. Esconjauregui, M. Fouquet, B.C. Bayer, C. Ducati, R. Smajda, S. Hofmann, J.
47 Robertson, Growth of ultrahigh density vertically aligned carbon nanotube forests for
48 interconnects, *ACS Nano*. 4 (2010) 7431-7436. <https://doi.org/10.1021/nn1025675>

- 1 [17] S.P. Patole, P.S. Alegaonkar, H.-C. Lee, J.-B. Yoo, Optimization of water assisted
2 chemical vapor deposition parameters for super growth of carbon nanotubes, *Carbon*. 46
3 (2008) 1987-1993. <https://doi.org/10.1016/j.carbon.2008.08.009>
- 4 [18] N. Suguru, H. Kei, S. Hisashi, K. Kazunori, Z. Zhengyi, M. Shigeo, Y. Yukio,
5 Millimeter-Thick Single-Walled Carbon Nanotube Forests: Hidden Role of Catalyst
6 Support, *Japanese Journal of Applied Physics*. 46 (2007) L399.
7 <https://doi.org/10.1143/JJAP.46.L399>
- 8 [19] C. Mattevi, C.T. Wirth, S. Hofmann, R. Blume, M. Cantoro, C. Ducati, C. Cepek, A.
9 Knop-Gericke, S. Milne, C. Castellarin-Cudia, S. Dolafi, A. Goldoni, R. Schloegl, J.
10 Robertson, In-situ X-ray Photoelectron Spectroscopy Study of Catalyst-Support
11 Interactions and Growth of Carbon Nanotube Forests, *The Journal of Physical Chemistry*
12 C. 112 (2008) 12207-12213. <https://doi.org/10.1021/jp802474g>
- 13 [20] P.B. Amama, C.L. Pint, S.M. Kim, L. McJilton, K.G. Eyink, E.A. Stach, R.H. Hauge, B.
14 Maruyama, Influence of Alumina Type on the Evolution and Activity of Alumina-
15 Supported Fe Catalysts in Single-Walled Carbon Nanotube Carpet Growth, *ACS Nano*. 4
16 (2010) 895-904. <https://doi.org/10.1021/nn901700u>
- 17 [21] S. Yasuda, D.N. Futaba, T. Yamada, J. Satou, A. Shibuya, H. Takai, K. Arakawa, M.
18 Yumura, K. Hata, Improved and Large Area Single-Walled Carbon Nanotube Forest
19 Growth by Controlling the Gas Flow Direction, *ACS Nano*. 3 (2009) 4164-4170.
20 <https://doi.org/10.1021/nn9007302>
- 21 [22] S. Sakurai, H. Nishino, D.N. Futaba, S. Yasuda, T. Yamada, A. Maigne, Y. Matsuo, E.
22 Nakamura, M. Yumura, K. Hata, Role of Subsurface Diffusion and Ostwald Ripening in
23 Catalyst Formation for Single-Walled Carbon Nanotube Forest Growth, *Journal of the*
24 *American Chemical Society*. 134 (2012) 2148-2153. <https://doi.org/10.1021/ja208706c>
- 25 [23] J.D. Beard, J. Stringer, O.R. Ghita, P.J. Smith, High Yield Growth of Patterned
26 Vertically Aligned Carbon Nanotubes Using Inkjet-Printed Catalyst, *ACS Applied*
27 *Materials & Interfaces*. 5 (2013) 9785-9790. <https://doi.org/10.1021/am402942q>
- 28 [24] K. Mizuno, K. Hata, T. Saito, S. Ohshima, M. Yumura, S. Iijima, Selective Matching of
29 Catalyst Element and Carbon Source in Single-Walled Carbon Nanotube Synthesis on
30 Silicon Substrates, *The Journal of Physical Chemistry B*. 109 (2005) 2632-2637.
31 <https://doi.org/10.1021/jp0454117>
- 32 [25] H. Nishino, S. Yasuda, T. Namai, D.N. Futaba, T. Yamada, M. Yumura, S. Iijima, K.
33 Hata, Water-Assisted Highly Efficient Synthesis of Single-Walled Carbon Nanotubes
34 Forests from Colloidal Nanoparticle Catalysts, *The Journal of Physical Chemistry C*. 111
35 (2007) 17961-17965. <https://doi.org/10.1021/jp0723719>
- 36 [26] E.S. Polsen, M. Bedewy, A.J. Hart, Decoupled Control of Carbon Nanotube Forest
37 Density and Diameter by Continuous-Feed Convective Assembly of Catalyst Particles,
38 *Small*. 9 (2013) 2564-2575. <https://doi.org/10.1002/sml.201202878>
- 39 [27] S. Dörfler, A. Meier, S. Thieme, P. Németh, H. Althues, S. Kaskel, Wet-chemical
40 catalyst deposition for scalable synthesis of vertical aligned carbon nanotubes on metal
41 substrates, *Chemical Physics Letters*. 511 (2011) 288-293.
42 <https://doi.org/10.1016/j.cplett.2011.06.027>
- 43 [28] H. Wang, C. Na, Chemical Bath Deposition of Aluminum Oxide Buffer on Curved
44 Surfaces for Growing Aligned Carbon Nanotube Arrays, *Langmuir*. 31 (2015) 7401-
45 7409. <https://doi.org/10.1021/acs.langmuir.5b01002>
- 46 [29] N.T. Alvarez, C.E. Hamilton, C.L. Pint, A. Orbaek, J. Yao, A.L. Frosinini, A.R. Barron,
47 J.M. Tour, R.H. Hauge, Wet Catalyst-Support Films for Production of Vertically Aligned
48 Carbon Nanotubes, *ACS Applied Materials & Interfaces*. 2 (2010) 1851-1856.
49 <https://doi.org/10.1021/am100128m>

- 1 [30] H. Wang, C. Na, Synthesis of millimeter-long vertically aligned carbon nanotube arrays
2 on aluminum oxide buffer prepared by layer-by-layer assembly of boehmite nanoplates,
3 Carbon. 66 (2014) 727-729. <https://doi.org/10.1016/j.carbon.2013.09.034>
- 4 [31] J.-M. Bonard, P. Chauvin, C. Klinke, Monodisperse Multiwall Carbon Nanotubes
5 Obtained with Ferritin as Catalyst, Nano Letters. 2 (2002) 665-667.
6 <https://doi.org/10.1021/nl0255606>
- 7 [32] L.Q. Fei L, Jia QX, Luo HM, Polymer-Assisted Deposition of Composite Catalysts for
8 the Growth of Vertical Aligned Carbon Nanotubes, Chem Eng Process Tech. 1 (2013)
9 1013.
- 10 [33] P.M. Parthangal, R.E. Cavicchi, M.R. Zachariah, A generic process of growing aligned
11 carbon nanotube arrays on metals and metal alloys, Nanotechnology. 18 (2007) 185605.
12 <https://doi.org/10.1088/0957-4484/18/18/185605>
- 13 [34] A. V. Naumkin, A. Kraut-Vass, S. W. Gaarenstroom, C. J. Powell, NIST X-ray
14 Photoelectron Spectroscopy Database, NIST Standard Reference Database 20, Version
15 4.1, U.S. Secretary of Commerce, (2012). <https://srdata.nist.gov/xps/>
- 16 [35] P.B. Amama, C.L. Pint, F. Mirri, M. Pasquali, R.H. Hauge, B. Maruyama, Catalyst-
17 support interactions and their influence in water-assisted carbon nanotube carpet growth,
18 Carbon. 50 (2012) 2396-2406. <https://doi.org/10.1016/j.carbon.2012.01.045>
- 19 [36] A. Kaneko, K. Yamada, R. Kumahara, H. Kato, Y. Homma, Comparative Study of
20 Catalytic Activity of Iron and Cobalt for Growing Carbon Nanotubes on Alumina and
21 Silicon Oxide, The Journal of Physical Chemistry C. 116 (2012) 26060-26065.
22 <https://doi.org/10.1021/jp309232w>
- 23 [37] M. Picher, H. Navas, R. Arenal, E. Quesnel, E. Anglaret, V. Jourdain, Influence of the
24 growth conditions on the defect density of single-walled carbon nanotubes, Carbon. 50
25 (2012) 2407-2416. <https://doi.org/10.1016/j.carbon.2012.01.055>
- 26 [38] C.L. Cheung, A. Kurtz, H. Park, C.M. Lieber, Diameter-Controlled Synthesis of Carbon
27 Nanotubes, The Journal of Physical Chemistry B. 106 (2002) 2429-2433.
28 <https://doi.org/10.1021/jp0142278>
- 29 [39] Y. Zhang, G. Zou, S.K. Doorn, H. Htoon, L. Stan, M.E. Hawley, C.J. Sheehan, Y. Zhu,
30 Q. Jia, Tailoring the Morphology of Carbon Nanotube Arrays: From Spinnable Forests to
31 Undulating Foams, ACS Nano. 3 (2009) 2157-2162. <https://doi.org/10.1021/nn9003988>
- 32 [40] C.S. Choi, J.E. Mapes, E. Prince, The structure of ammonium nitrate (IV), Acta
33 Crystallogr. B28 (1972) 1357-1361. <https://doi.org/10.1107/S0567740872004303>
- 34 [41] A. Yamamoto, Modulated structure of wustite (Fe_{1-x}O) (three-dimensional modulation),
35 Acta Crystallogr. B38 (1982) 1451-1456. <https://doi.org/10.1107/S056774088200613X>

36